GMTI Tracking using Signal Strength Information

Michael Mertens
Dept. Sensor Data and Information Fusion
Fraunhofer FKIE
Wachtberg, Germany
michael.mertens@fkie.fraunhofer.de

Martin Ulmke
Dept. Sensor Data and Information Fusion
Fraunhofer FKIE
Wachtberg, Germany
martin.ulmke@fkie.fraunhofer.de

Abstract – *Signal strength information is a standard output of a modern radar system. Provided the amplitude of the target returns exceeds the false alarm background, the consideration of signal strength may lead to improved target estimates, depending on the scenario. In this paper a Bayesian tracking algorithm is presented which incorporates the signal strength information. In contrast to previous approaches, the knowledge on the target's signal strength is not only used for an improved calculation of the association probabilities, but it enters into the algorithm as a random variable which is sequentially estimated. By this approach it is not only possible to discriminate closely-spaced targets and improve the track continuity, but also to support possible classification and identification tasks. The signal strength fluctuations of the target returns are modeled by the Swerling-I and Swerling-III cases. As a first performance evaluation, numerical results are presented based on a multi-target simulation scenario.*

Keywords: Ground moving target indication (GMTI), target tracking, signal strength, Swerling fluctuation models.

1 Introduction

In ground surveillance with airborne Ground Moving Target Indication (GMTI) radar, the main task of establishing and maintaining tracks of relevant moving objects is challenged not only by imprecise, uncertain and ambiguous measurements. To a large degree, the main difficulty arises from complex target dynamics, e.g. stop & go behavior or strong maneuvers, masking due to the sensors Doppler blind zone, nontrivial topography causing terrain obscuration, situations with closely-spaced targets, a strong false alarm background, etc. In general, these factors quickly lead to a strong performance degradation or even track loss. To counterbalance these factors, it is beneficial to incorporate additional sources of information into the tracking process. In this work, we focus on the impact of the received signal strength of a target on the tracking performance.

Being a standard output of a modern radar system, the target amplitude or the corresponding target signal strength has already been used in the past to facilitate the problem of associating a track with its correct measurement. But in contrast to previous approaches, e.g. [1, 2, 3], in this work the knowledge on the target's signal strength is not only used for an improved calculation of the association probabilities, but it enters into the algorithm as a random variable which is sequentially estimated. By this approach it is not only possible to discriminate closely-spaced targets and improve the track continuity, but also to support possible subsequent classification and identification tasks. In addition, for phased array antennas the signal strength estimates could also be used to contribute to the radar resource management: Depending on the estimated target SNR, the detection threshold could be adapted to allow better target detections.

The paper is organized as follows: The next part briefly describes the target fluctuation models and the detection process assumed in this work. In part 3 the tracking algorithm is presented which incorporates the signal strength information, followed by the discussion of the simulation scenario and Monte Carlo results. Throughout the paper, a linear scale is used for signal strength values.

2 Signal strength model

2.1 Target fluctuations

Due to its complexity, a realistic modelling of a real target's back-scattering characteristics is in general impossible. Therefore statistical models are used instead which can be handled analytically. In this work it is assumed that the fluctuations of the input signal at the detector, resulting from fluctuations of the target cross section, can be described by the Swerling models [4]. The statistical properties of chi-square target fluctuations are determined by the following general proba-

bility density which depends on the average signal-to-noise ratio, SNR_0, and the parameter m, which indicates the degrees of freedom ($2m$) of the associated chi-square distribution:

$$\mathcal{G}^m_{\mathrm{SNR}_0}(\mathrm{SNR}) = \frac{(m/\mathrm{SNR}_0)^m}{\Gamma(m)} \mathrm{SNR}^{m-1} e^{-m\mathrm{SNR}/\mathrm{SNR}_0} \quad (1)$$

Assuming independent fluctuations from scan to scan, the relevant Swerling cases are given by $m = 1$ (Swerling-I) and $m = 2$ (Swerling-III):

$$\mathcal{G}^1_{\mathrm{SNR}_0}(\mathrm{SNR}) = \frac{1}{\mathrm{SNR}_0} e^{-\mathrm{SNR}/\mathrm{SNR}_0} \quad (2)$$

$$\mathcal{G}^2_{\mathrm{SNR}_0}(\mathrm{SNR}) = \frac{4\mathrm{SNR}}{\mathrm{SNR}_0^2} e^{-2\,\mathrm{SNR}/\mathrm{SNR}_0} \quad (3)$$

2.2 Detection process

The complex target signal $\mathbf{v} = (v_1, v_2)$ with orthogonal and statistically independent components is added by white Gaussian noise within the receiver unit. The detector uses the total signal $\mathbf{u} = (u_1, u_2)$ to form the signal strength $||\mathbf{u}||^2 = (u_1)^2 + (u_2)^2$ with the probability density given by the Rice distribution

$$p(||\mathbf{u}||^2|\mathbf{v}) = \frac{1}{2\sigma_n^2} e^{-\frac{||\mathbf{u}||^2+||\mathbf{v}||^2}{2\sigma_n^2}} I_0\left(\frac{||\mathbf{u}|| \cdot ||\mathbf{v}||}{\sigma_n^2}\right) \quad (4)$$

where I_0 denotes the modified Bessel function of the first kind. Normalized to the mean noise level, $\mathrm{E}[p(||\mathbf{u}||^2|0)] = 2\sigma_n^2$, i.e. with $s = ||\mathbf{u}||^2/2\sigma_n^2$ and $\mathrm{SNR} = ||\mathbf{v}||^2/2\sigma_n^2$, this can be rewritten as

$$p(s|\mathrm{SNR}) = e^{-s-\mathrm{SNR}} I_0\left(2\sqrt{s} \cdot \sqrt{\mathrm{SNR}}\right) \quad (5)$$

with expectation value $\mathrm{E}[s] = 1 + \mathrm{SNR}$ and thus unit power for noise (SNR=0). Following the assumption from the last section, the signal-to-noise ratio SNR itself fluctuates with mean SNR_0. Thus the overall received signal strength is derived by

$$p(s|\mathrm{SNR}_0) = \int_0^\infty d\mathrm{SNR}\; p(s|\mathrm{SNR})\, p(\mathrm{SNR}|\mathrm{SNR}_0) \quad (6)$$

with $p(\mathrm{SNR}|\mathrm{SNR}_0)$ given by $\mathcal{G}^m_{\mathrm{SNR}_0}(\mathrm{SNR})$. Finally one ends up with the well-known distributions for the two Swerling cases:

$$p(s|\mathrm{SNR}_0, m=1) = \frac{1}{1+\mathrm{SNR}_0} e^{-s/(1+\mathrm{SNR}_0)} \quad (7)$$

$$p(s|\mathrm{SNR}_0, m=2) = \frac{1}{(1+\mathrm{SNR}_0/2)^2} e^{-s/(1+\mathrm{SNR}_0/2)} \cdot \left[1 + \frac{s}{1+2/\mathrm{SNR}_0}\right] \quad (8)$$

As soon as signal strength is considered, the detection probability is no longer a parameter but becomes a function of the target's mean signal-to-noise ratio SNR_0 and the detection threshold λ:

$$\mathbf{P}(s > \lambda|D) = \mathbf{P}_D(\mathrm{SNR}_0, \lambda, m) = \int_\lambda^\infty ds\; p(s|\mathrm{SNR}_0, m) \quad (9)$$

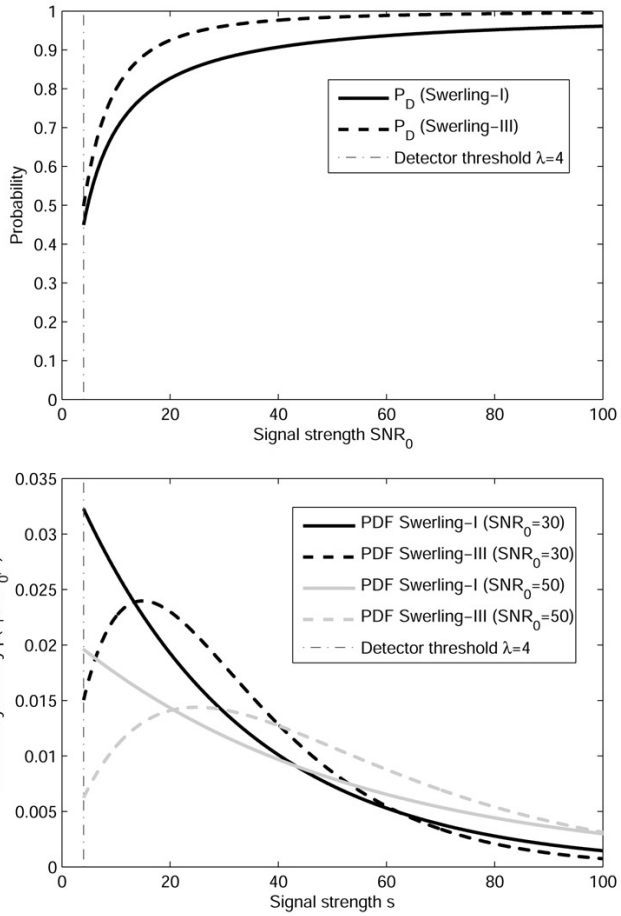

Figure 1: Distributions of the detection probability (upper plot) and probability density (bottom) for the Swerling-I and Swerling-III models.

where D denotes detection. For the two Swerling models, the integration yields the corresponding detection probabilities, see Fig. (1):

$$\mathbf{P}^{\mathbf{I}}_D = e^{-\lambda/(1+\mathrm{SNR}_0)} \quad (10)$$

$$\mathbf{P}^{\mathbf{III}}_D = e^{-\lambda/(1+\mathrm{SNR}_0/2)} \left[1 + \frac{\lambda \cdot \mathrm{SNR}_0/2}{(1+\mathrm{SNR}_0/2)^2}\right] \quad (11)$$

Detections are only available, if the signal strength of the input signal exceeds the detection threshold. Thus the probability densities (7) and (8) need to be normalized properly, yielding for $s \geq \lambda$

$$p(s|\mathrm{SNR}_0, \lambda, \mathbf{I}) = \frac{1}{\mathbf{P}^{\mathbf{I}}_D}\, p(s|\mathrm{SNR}_0, m=1) \quad (12)$$

$$p(s|\mathrm{SNR}_0, \lambda, \mathbf{III}) = \frac{1}{\mathbf{P}^{\mathbf{III}}_D}\, p(s|\mathrm{SNR}_0, m=2) \quad (13)$$

These distributions are plotted in Fig. (1) for different values of SNR_0. Measurements which originate from false alarms are modelled by the Swerling-I case, i.e.

$$p(s|\mathrm{CNR}_0) = \frac{1}{\mathbf{P}^{\mathbf{I}}_D(\mathrm{CNR}_0)} \frac{e^{-s/(1+\mathrm{CNR}_0)}}{1+\mathrm{CNR}_0} \quad (14)$$

if $s \geq \lambda$ with CNR_0 being the mean clutter strength-to-noise ratio. It is assumed that the detection threshold λ on the input signal power is high enough to suppress measurements resulting from receiver noise.

3 Incorporation of signal strength information

In Bayesian target tracking, e.g. [5, 6], the probability density $p(\mathbf{x}_k|\mathcal{Z}^k)$, which describes the target state $\mathbf{x}_k$ at time step t_k, conditioned on the measurement sequence $\mathcal{Z}^k = \{\mathbf{z}_1, \mathbf{z}_2, ..., \mathbf{z}_k\}$ with $\mathbf{z}_k = \{z_k^i\}_{i=1}^{n_k}$, is sequentially updated by

$$p(\mathbf{x}_k|\mathcal{Z}^k) = \frac{p(\mathbf{z}_k|\mathbf{x}_k)\, p(\mathbf{x}_k|\mathcal{Z}^{k-1})}{\int d\mathbf{x}_k\, p(\mathbf{z}_k|\mathbf{x}_k)\, p(\mathbf{x}_k|\mathcal{Z}^{k-1})} \tag{15}$$

To incorporate signal strength, the random variable $\mathbf{s}_k$ is introduced, thus the target state becomes $\mathbf{X}_k = (\mathbf{x}_k, \mathbf{s}_k)$ and $\mathbf{Z}_k = \{z_k^i, \kappa_k^i\}_{i=1}^{n_k}$ with signal strength measurements κ_k^i. It follows

$$p(\mathbf{X}_k|\mathcal{Z}^k) = \frac{p(\mathbf{Z}_k|\mathbf{X}_k)\, p(\mathbf{X}_k|\mathcal{Z}^{k-1})}{\int d\mathbf{x}_k d\mathbf{s}_k\, p(\mathbf{Z}_k|\mathbf{X}_k)\, p(\mathbf{X}_k|\mathcal{Z}^{k-1})} \tag{16}$$

In the following, expressions for the prior density $p(\mathbf{X}_k|\mathcal{Z}^{k-1})$ and the likelihood function $p(\mathbf{Z}_k|\mathbf{X}_k)$ will be derived.

3.1 Prediction step

First of all, the density $p(\mathbf{X}_k|\mathcal{Z}^{k-1})$ can be split up into the kinematic and the signal strength part:

$$p(\mathbf{X}_k|\mathcal{Z}^{k-1}) = p(\mathbf{s}_k|\mathbf{x}_k, \mathcal{Z}^{k-1})\, p(\mathbf{x}_k|\mathcal{Z}^{k-1}) \tag{17}$$

The kinematic prior is treated in a traditional way: A Gaussian shaped posterior density $p(\mathbf{x}_{k-1|k-1}|\mathcal{Z}^{k-1})$ is assumed which is propagated to the actual time step t_k by utilizing a linear dynamics model with additive white Gaussian noise. This yields

$$p(\mathbf{x}_k|\mathcal{Z}^{k-1}) = \mathcal{N}(\mathbf{x}_k; \mathbf{x}_{k|k-1}, \mathbf{P}_{k|k-1}) \tag{18}$$

where the estimate $\mathbf{x}_{k|k-1}$ and covariance $\mathbf{P}_{k|k-1}$ are given by the known Kalman prediction equations.
On the other hand, the prior density of the signal strength has to account for the fact that the target's mean signal-to-noise ratio SNR_0 is an a-priori unknown but assumed constant value. Thus for $p(\mathbf{s}_k|\mathbf{x}_k, \mathcal{Z}^{k-1})$ a class of densities should be chosen which, up to a normalization constant, is invariant under the successive application of Bayes equation (16). Following [7], the class of inverse Gamma densities $\mathcal{I}(s; \hat{s}, \mu)$ is chosen which guarantees the aforementioned behavior:

$$p(\mathbf{s}_k|\mathbf{x}_k, \mathcal{Z}^{k-1}) = \mathcal{I}(\mathbf{s}_k; \hat{\mathbf{s}}_{k-1}, \mu_{k-1}) \tag{19}$$

$$= \text{N}_{\mu_{k-1}} \mathbf{s}_k^{-\mu_{k-1}-1} e^{-\frac{(\mu_{k-1}-1)\hat{\mathbf{s}}_{k-1}}{\mathbf{s}_k}} \tag{20}$$

with normalization constant

$$\text{N}_{\mu_{k-1}} = \frac{[(\mu_{k-1}-1)\hat{\mathbf{s}}_{k-1}]^{\mu_{k-1}}}{\Gamma(\mu_{k-1})} \tag{21}$$

The distribution of the inverse Gamma density is shown in Fig. 2. The probability density $\mathcal{I}(\mathbf{s}; \hat{\mathbf{s}}, \mu)$ has the expectation value $\text{E}[\mathbf{s}] = \hat{\mathbf{s}}$. If the parameter $\mu > 2$, then the variance exists with $\text{Var}[\mathbf{s}] = \frac{\mathbf{s}^2}{\mu-2}$. Because of $\frac{d}{dt}\text{SNR}_0 = 0$, no "dynamics" is needed for the signal strength, thus the prior density at t_k is identical to the posterior density at t_{k-1}:

$$\mathcal{I}(\mathbf{s}_k; \hat{\mathbf{s}}_{k-1}, \mu_{k-1}) = \mathcal{I}(\mathbf{s}_k; \mathbf{s}_{k-1|k-1}, \mu_{k-1|k-1}) \tag{22}$$

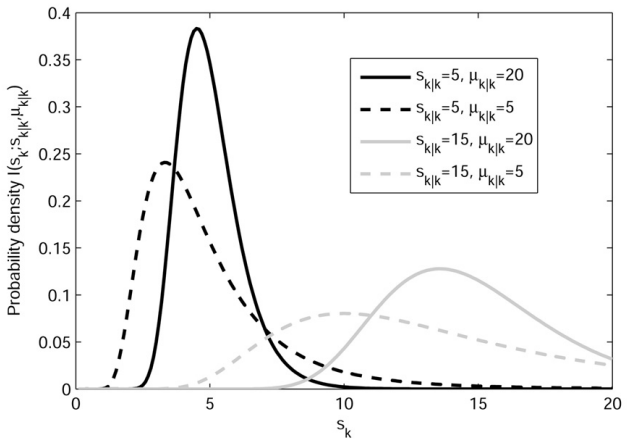

Figure 2: Distribution of the inverse Gamma density $\mathcal{I}(\mathbf{s}_k; \mathbf{s}_{k|k}, \mu_{k|k})$.

3.2 Combined likelihood

The combined likelihood function $p(\mathbf{Z}_k|\mathbf{X}_k) = p(\mathbf{Z}_k|\mathbf{x}_k, \mathbf{s}_k)$ is the probability density of the measurements and comprises all possibilities how the given sensor output $\mathbf{Z}_k$ can be interpreted, given the true target state $\mathbf{X}_k$. Assuming independent, identically distributed false alarm measurements with the number of false alarms determined by the Poisson distribution, the likelihood function, up to a factor which does not depend on $\mathbf{X}_k$, can be written as

$$p(\mathbf{Z}_k|\mathbf{X}_k) \propto (1 - \mathbf{P}_D(\mathbf{s}_k))\rho_F + \mathbf{P}_D(\mathbf{s}_k) \sum_{i=1}^{n_k} \mathcal{N}(z_k^i; \mathbf{H}_k\mathbf{x}_k, \mathbf{R}_k)\, \mathcal{LR}_S^i \tag{23}$$

where ρ_F is the false alarm density and $\mathcal{N}(z_k^i; \mathbf{H}_k\mathbf{x}_k, \mathbf{R}_k)$ is the normally distributed single measurement likelihood, which results from a linear measurement model with additive white Gaussian noise: $z_k^i = \mathbf{H}_k\mathbf{x}_k + v_k$, $\mathbf{v}_k \propto \mathcal{N}(\mathbf{v}_k; 0, \mathbf{R}_k)$ with measurement matrix $\mathbf{H}_k$ and measurement covariance

$\mathbf{R}_k$. The signal strength likelihood ratio $\mathcal{LR}_S^i$ in (23) is given by

$$\mathcal{LR}_S^i = \frac{p(\kappa_k^i|i, D, \mathbf{X}_k)}{p(\kappa_k^i|\neg D, \mathbf{X}_k)} \tag{24}$$

where $(D, \neg D)$ describe detection and missed detection, respectively. $p(\kappa_k^i|\neg D, \mathbf{X}_k)$ is given by (14) and $p(\kappa_k^i|i, D, \mathbf{X}_k)$ is distributed according to either (12) or (13). In the latter case, the detection probability is approximated by the Swerling-I case, i.e. $\mathbf{P}_D^{\mathbf{III}} \approx \mathbf{P}_D^{\mathbf{I}}$. Finally, the combined likelihood can be calculated, yielding

Swerling-I:

$$p(\mathbf{Z}_k|\mathbf{X}_k) \propto (1 - e^{-\frac{\lambda}{1+\mathbf{s}_k}})\rho_F + \sum_{i=1}^{n_k} \alpha_{\mathbf{c}_k}^i \frac{e^{-\kappa_k^i/(1+\mathbf{s}_k)}}{1+\mathbf{s}_k} \mathcal{N}(z_k^i; \mathbf{H}_k\mathbf{x}_k, \mathbf{R}_k) \tag{25}$$

Swerling-III:

$$p(\mathbf{Z}_k|\mathbf{X}_k) \propto (1 - e^{-\frac{\lambda}{1+\mathbf{s}_k}})\rho_F + \sum_{i=1}^{n_k} \left[4\alpha_{\mathbf{c}_k}^i \frac{e^{-2\kappa_k^i/(2+\mathbf{s}_k)}}{(2+\mathbf{s}_k)^2} \cdot \left(1 + \frac{\kappa_k^i \mathbf{s}_k}{2+\mathbf{s}_k}\right) \mathcal{N}(z_k^i; \mathbf{H}_k\mathbf{x}_k, \mathbf{R}_k) \right] \tag{26}$$

with

$$\alpha_{\mathbf{c}_k}^i = (1 + \mathbf{c}_k)\, e^{\frac{\kappa_k^i - \lambda}{1+\mathbf{c}_k}} \tag{27}$$

3.3 Filter update step

The posterior density $p(\mathbf{X}_k|\mathcal{Z}^k) = p(\mathbf{x}_k, \mathbf{s}_k|\mathcal{Z}^k)$ is derived by inserting the prediction and likelihood functions into (16), assuming strong targets, i.e. $1 + \mathbf{s}_k \approx 2 + \mathbf{s}_k \approx \mathbf{s}_k$, and making use of the product formula for normal distributions [8]. The result is a weighted sum of the product of a Gaussian with an inverse Gamma density, describing the target's kinematic state and signal strength, respectively:

$$p(\mathbf{X}_k|\mathcal{Z}^k) = \sum_{i=0}^{n_k} w_k^i \, \mathcal{N}(\mathbf{x}_k; \mathbf{x}_{k|k}^i, \mathbf{P}_{k|k}^i) \, \mathcal{I}(\mathbf{s}_k; \mathbf{s}_{k|k}^i, \mu_{k|k}^i) \tag{28}$$

where the estimates $\mathbf{x}_{k|k}^i$ and covariances $\mathbf{P}_{k|k}^i$ are calculated by the known Kalman filter update equations, and weights w_k^i, signal strength estimates $\mathbf{s}_{k|k}^i$ and $\mu_{k|k}^i$ are given by (for $i > 0$)

Swerling-I:

$$\tilde{w}_k^i = \frac{\alpha_{\mathbf{c}_k}^i}{\rho_F} \mathcal{N}(z_k^i; \mathbf{H}_k\mathbf{x}_{k|k-1}, \mathbf{S}_k^i) \frac{\mu_{k-1}}{(\mu_{k-1}-1)\hat{\mathbf{s}}_{k-1}} \cdot \left[\frac{(\mu_{k-1}-1)\hat{\mathbf{s}}_{k-1}}{(\mu_{k-1}-1)\hat{\mathbf{s}}_{k-1} + \kappa_k^i}\right]^{\mu_{k-1}+1} \tag{29}$$

$$\mathbf{s}_{k|k}^i = \frac{\mu_{k-1}-1}{\mu_{k-1}} \hat{\mathbf{s}}_{k-1} + \frac{\kappa_k^i}{\mu_{k-1}} \tag{30}$$

$$\mu_{k|k}^i = \mu_{k-1} + 1 \tag{31}$$

Swerling-III:

$$\tilde{w}_k^i = \frac{4\alpha_{\mathbf{c}_k}^i}{\rho_F} \mathcal{N}(z_k^i; \mathbf{H}_k\mathbf{x}_{k|k-1}, \mathbf{S}_k^i) \cdot \frac{(1+\kappa_k^i)\mu_{k-1}(\mu_{k-1}+1)}{[(\mu_{k-1}-1)\hat{\mathbf{s}}_{k-1}]^2} \cdot \left[\frac{(\mu_{k-1}-1)\hat{\mathbf{s}}_{k-1}}{(\mu_{k-1}-1)\hat{\mathbf{s}}_{k-1} + 2\kappa_k^i}\right]^{\mu_{k-1}+2} \tag{32}$$

$$\mathbf{s}_{k|k}^i = \frac{\mu_{k-1}-1}{\mu_{k-1}+1} \hat{\mathbf{s}}_{k-1} + \frac{2\kappa_k^i}{\mu_{k-1}+1} \tag{33}$$

$$\mu_{k|k}^i = \mu_{k-1} + 2 \tag{34}$$

and for the missed detection hypothesis ($i = 0$)

$$\tilde{w}_k^0 = 1 - \left[\frac{\hat{\mathbf{s}}_{k-1}}{\hat{\mathbf{s}}_{k-1} + \frac{\lambda}{\mu_{k-1}-1}}\right]^{\mu_{k-1}} \tag{35}$$

$$\mathbf{s}_{k|k}^0 = \frac{1}{\tilde{w}_k^0} \left(\hat{\mathbf{s}}_{k-1} - \left[\frac{\hat{\mathbf{s}}_{k-1}}{\hat{\mathbf{s}}_{k-1} + \frac{\lambda}{\mu_{k-1}-1}}\right]^{\mu_{k-1}} \mathbf{s}_{k|k}^* \right) \tag{36}$$

$$\mu_{k|k}^0 = \frac{(\mathbf{s}_{k|k}^0)^2}{\mathrm{Var}[\mathbf{s}_{k|k}^0]} + 2 \tag{37}$$

with

$$w_k^i = \frac{\tilde{w}_k^i}{\sum_{j=0}^{n_k} \tilde{w}_k^i} \tag{38}$$

$$\alpha_{\mathbf{c}_k}^i = (1 + \mathbf{c}_k) e^{\frac{\kappa_k^i - \lambda}{1+\mathbf{c}_k}} \tag{39}$$

$$\mathbf{s}_{k|k}^* = \hat{\mathbf{s}}_{k-1} + \frac{\lambda}{\mu_{k-1}-1} \tag{40}$$

$$\mathrm{Var}[\mathbf{s}_{k|k}^0] = \frac{1}{\tilde{w}_k^0} \left[\left(\frac{(\hat{\mathbf{s}}_{k-1})^2}{\mu_{k-1}-2} \right) + (\hat{\mathbf{s}}_{k-1} - \mathbf{s}_{k|k}^0)^2 \right] - \frac{1}{\tilde{w}_k^0} \left(\frac{\hat{\mathbf{s}}_{k-1}}{\hat{\mathbf{s}}_{k-1} + \frac{\lambda}{\mu_{k-1}-1}} \right)^{\mu_{k-1}} \cdot \left[\left(\frac{(\mathbf{s}_{k|k}^*)^2}{\mu_{k-1}-2} \right) + (\mathbf{s}_{k|k}^* - \mathbf{s}_{k|k}^0)^2 \right] \tag{41}$$

The update equations for $\mathbf{s}_{k|k}^i$ and $\mu_{k|k}^i$ exhibit a reasonable behavior: The expectation of the prior density, $\hat{\mathbf{s}}_{k-1}$, is modified by the measurement κ_k^i and the variance $\mathrm{Var}[\mathbf{s}_{k|k}^i] = (\mathbf{s}_{k|k}^i)^2/(\mu_{k|k}^i - 2)$ decreases with time as $\mu_{k|k}^i$ increases. Due to the factor $(1 - e^{-\lambda/1+\mathbf{s}_k})$ in (25) and (26), the missed detection hypothesis splits up into two components which are processed by second-order moment matching [5] resulting in a single merged component with $\tilde{w}_k^0$, $\mathbf{s}_{k|k}^0$ and $\mu_{k|k}^0$ as given above.

3.4 Algorithmic implementation

The presented update scheme is implemented into the single-target PDAF [5] and the multi-target JPDAF [6] tracking algorithms. In the PDAF algorithm, n_k measurements lead to $n_k + 1$ hypotheses which are merged to a single main hypothesis by second-order moment

matching at the end of the filter update step. In this case, the implementation is straightforward, because the derived update equations from the last section can be used directly without any further adjustments.
In the JPDAF algorithm, the complete set of possible global hypotheses is processed, i.e. all possible combinations to associate measurements to tracks including missed detections and false alarms are considered. Thus it avoids the association of a certain measurement to more than one track, which is a shortcoming of the simple single-target PDAF. In this case, adjustments need to be made because the individual association probabilities for each target with its relevant measurements are calculated based on the probabilities of the global hypotheses, and are not given by (29), (32) and (35). Therefore, the calculation of the probability of the global hypotheses needs to be adapted to account for the weight factors due to the signal strength incorporation. This is done in the folowing way:
In the original formulation of the JPDAF, the probability of the global hypothesis θ_i is given by

$$P(\theta_i|\mathcal{Z}^k) = \prod_{i=1}^{n_k} \left\{ \frac{1}{\rho_F} \mathcal{N}(z_k^i; \mathbf{H}_k \mathbf{x}_{k|k-1}^{t_i}, \mathbf{S}_k^{t_i}) \right\}^{\tau_i} \cdot \prod_{t=1}^{T} \mathbf{P}_D^{\delta_t} \left(1 - \mathbf{P}_D\right)^{1-\delta_t} \quad (42)$$

where $\tau_i \in \{0,1\}$ indicates if measurement i is associated with target t_i, and $\delta_t \in \{0,1\}$ indicates if target t is associated with a measurement. First of all, $\mathbf{P}_D^{\delta_t}$ can be shifted into the first product (dropping the index δ_t). Now the factor

$$\frac{\mathbf{P}_D}{\rho_F} \mathcal{N}(z_k^i; \mathbf{H}_k \mathbf{x}_{k|k-1}^{t_i}, \mathbf{S}_k^{t_i}) \quad (43)$$

is replaced by (29) for Swerling-I and (32) for Swerling-III. In addition, the probability factor for the missed detection hypothesis, $1 - \mathbf{P}_D$, is replaced by (35). With these adjustments, $P(\theta_i|\mathcal{Z}^k)$ can be written as

Swerling-I:

$$P(\theta_i|\mathcal{Z}^k) = \prod_{i=1}^{n_k} \left\{ \frac{\alpha_{\mathbf{c}_k}^i}{\rho_F} \frac{\mu_{k-1}}{(\mu_{k-1}-1)\hat{\mathbf{s}}_{k-1}} \cdot \left[\frac{(\mu_{k-1}-1)\hat{\mathbf{s}}_{k-1}}{(\mu_{k-1}-1)\hat{\mathbf{s}}_{k-1} + \kappa_k^i} \right]^{\mu_{k-1}+1} \cdot \mathcal{N}(z_k^i; \mathbf{H}_k \mathbf{x}_{k|k-1}^{t_i}, \mathbf{S}_k^{t_i}) \right\}^{\tau_i} \cdot \prod_{t=1}^{T} \left(1 - \left[\frac{\hat{\mathbf{s}}_{k-1}}{\hat{\mathbf{s}}_{k-1} + \frac{\lambda}{\mu_{k-1}-1}} \right]^{\mu_{k-1}} \right)^{1-\delta_t} \quad (44)$$

and

Swerling-III:

$$P(\theta_i|\mathcal{Z}^k) = \prod_{i=1}^{n_k} \left\{ \frac{4\alpha_{\mathbf{c}_k}^i}{\rho_F} \frac{(1+\kappa_k^i)\mu_{k-1}(\mu_{k-1}+1)}{[(\mu_{k-1}-1)\hat{\mathbf{s}}_{k-1}]^2} \cdot \left[\frac{(\mu_{k-1}-1)\hat{\mathbf{s}}_{k-1}}{(\mu_{k-1}-1)\hat{\mathbf{s}}_{k-1} + 2\kappa_k^i} \right]^{\mu_{k-1}+2} \cdot \mathcal{N}(z_k^i; \mathbf{H}_k \mathbf{x}_{k|k-1}^{t_i}, \mathbf{S}_k^{t_i}) \right\}^{\tau_i} \cdot \prod_{t=1}^{T} \left(1 - \left[\frac{\hat{\mathbf{s}}_{k-1}}{\hat{\mathbf{s}}_{k-1} + \frac{\lambda}{\mu_{k-1}-1}} \right]^{\mu_{k-1}} \right)^{1-\delta_t} \quad (45)$$

From that, the individual association probabilities for each target are calculated in the same way as in the original JPDAF.

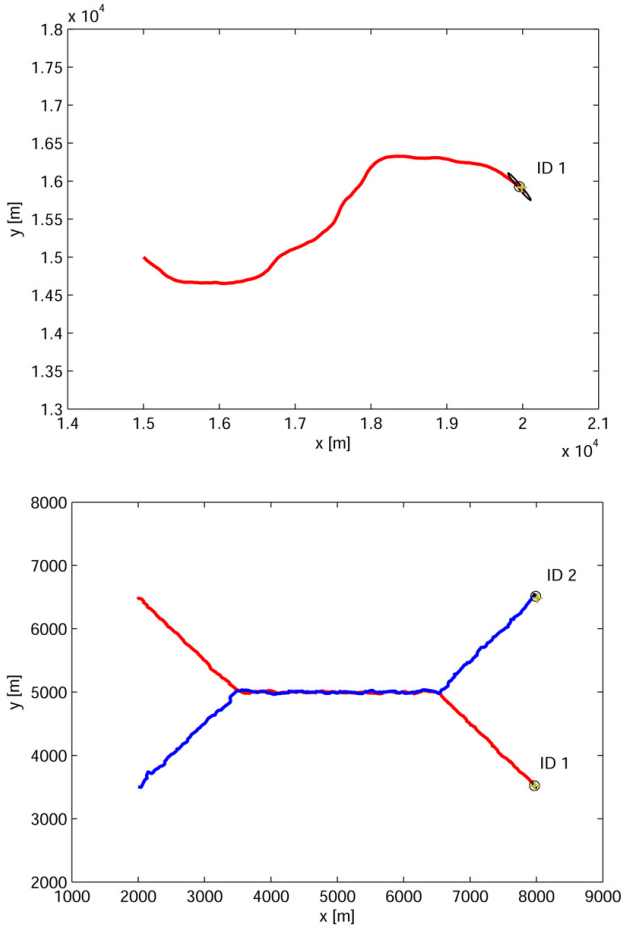

Figure 3: Single-target (above) and two-target (bottom) simulation scenarios. Shown is the snapshot at the final revisit time.

4 Simulation scenario & results

As a first performance evaluation, the algorithm presented in the last section is applied to a single-target and a two-target scenario with the trajectories shown

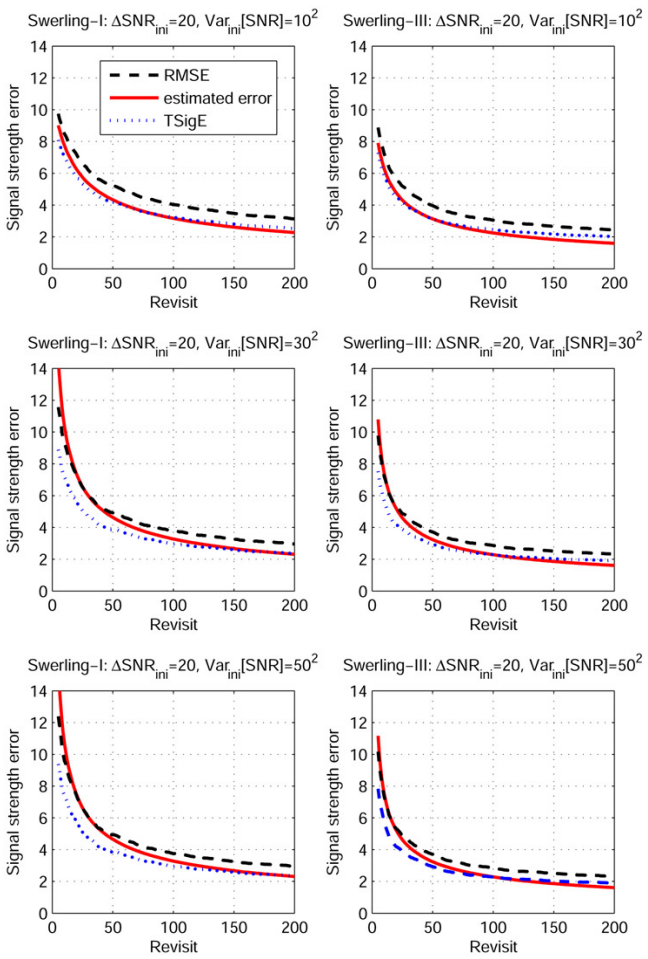

Figure 4: Monte Carlo results for initialization with $\text{SNR}_{ini} \in [\text{SNR}_0 - 20, \text{SNR}_0 + 20]$ where $\text{SNR}_0 = 30$. The results correspond to Swerling-I (left column) and Swerling-III (right column).

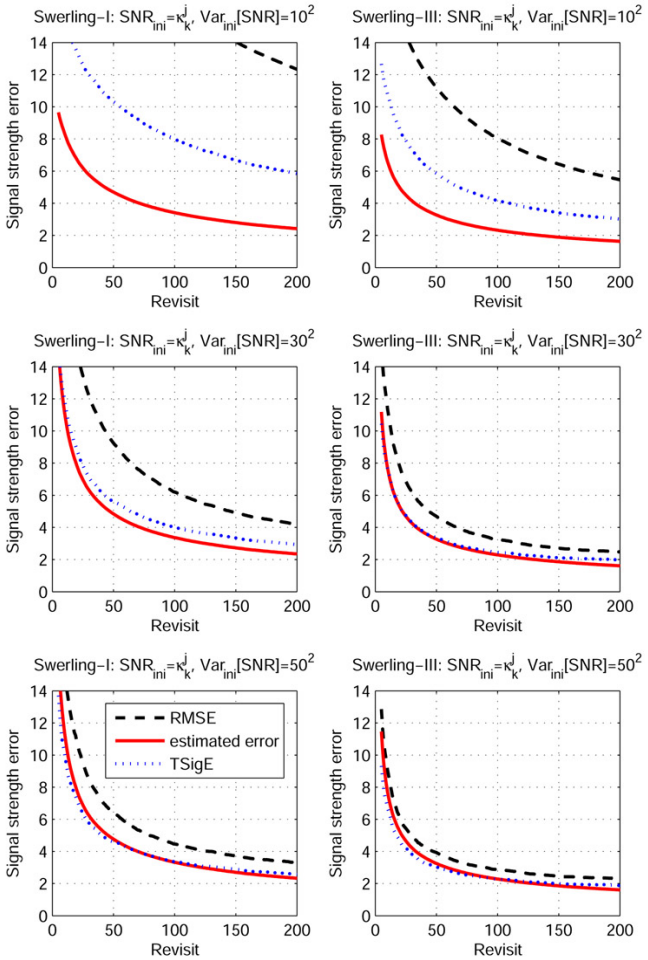

Figure 5: Monte Carlo results for initialization with the first signal strength measurement, $\text{SNR}_{ini} = \kappa_0^j$. The results correspond to Swerling-I (left column) and Swerling-III (right column).

in Fig. 3. For the Monte Carlo analysis, the highly fluctuating signal strength measurements are created based on the inversion method [9] for Swerling-I and the acceptance-rejection method [9] for Swerling-III. All results are based on 1000 Monte Carlo runs.

In the first scenario, the objective is to analyze the important question of track initialization of the signal strength component, i.e. the parameter sensitivity and convergence. In order to quantify the results, the following errors are calculated: The signal strength root mean square error (RMSE), the target signal strength error (TSigE), given by

$$\text{TSigE}(k) = \frac{1}{N_{MC}} \sum_{n=1}^{N_{MC}} \left(s_{k|k}^n - \text{SNR}_0 \right) \qquad (46)$$

and the error from the estimated variance. The signal strength component is initialized either with a randomly chosen value from an interval around the true signal strength SNR_0, $\text{SNR}_{ini} \in [\text{SNR}_0 - \Delta\text{SNR}_{ini}, \text{SNR}_0 + \Delta\text{SNR}_{ini}]$ (case 1). This corresponds to the case if the true value is not known, but at least some approximate knowledge from, e.g, a preceding signal processing step is already available. Or the signal strength is initialized simply with the first available measurement in close analogy to the initialization of the kinematic component (case 2). The evolution of the above mentioned signal strength errors for these two possibilities are shown in Fig. 4 with $\text{SNR}_0 = 30$, $\Delta\text{SNR}_{ini} = 20$ and Fig. 5, respectively, based on the PDAF algorithm and the simulation parameters given in Tab. 1. Different rows correspond to different initial values of the signal strength variance Var_{ini}, and the columns correspond to Swerling-I and Swerling-III, respectively. As expected, in all cases the RMSE is larger than the TSigE, because the RMSE penalizes larger deviations from the true value more severely due to the mean square. If the initialization is carried out based on case 1, all possible values of the initial variance lead to stable signal strength estimates with good convergence behav-

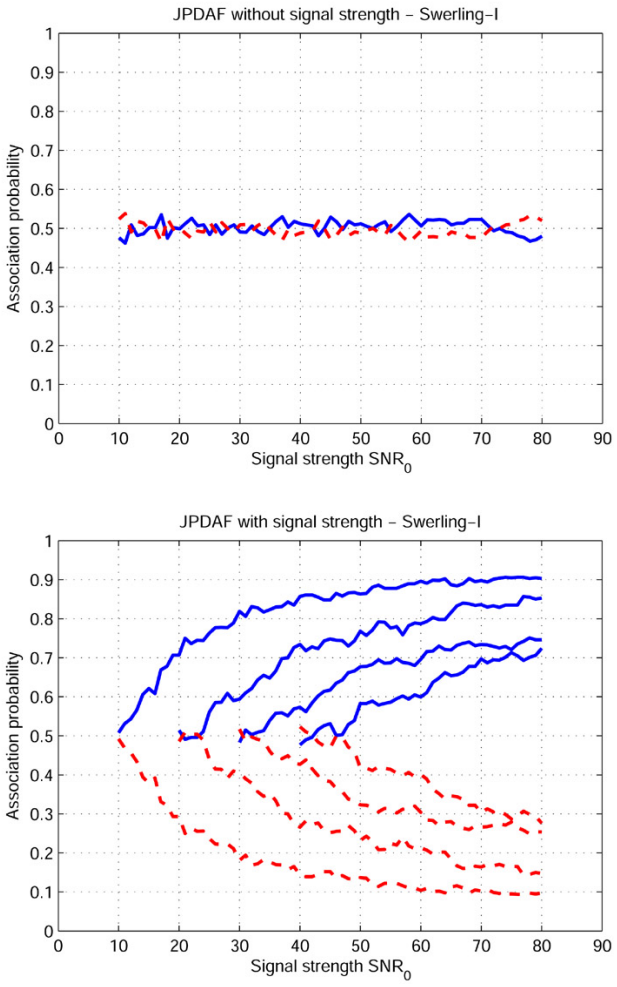

Figure 6: Probability for correct (solid lines) and incorrect (dashed lines) association of tracks with true targets at final revisit for different signal strength combinations, based on fluctuation model Swerling-I. The signal strength of one target is fix, corresponding to the minimum value of each line. Shown are the results for JPDAF without (above) and with (below) exploitation of signal strength information.

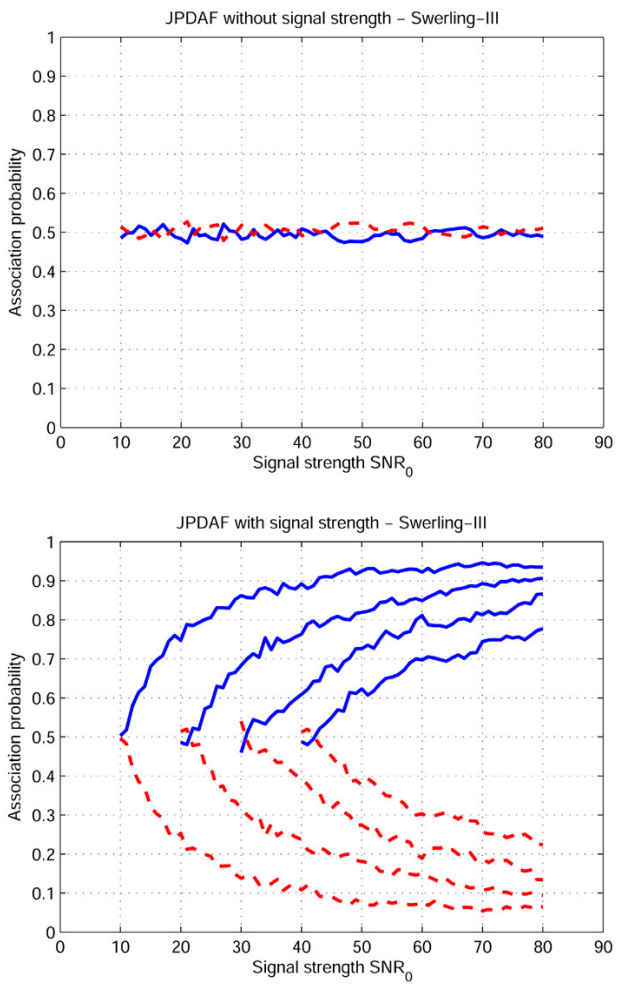

Figure 7: Probability for correct (solid lines) and incorrect (dashed lines) association of tracks with true targets at final revisit for different signal strength combinations, based on fluctuation model Swerling-III. The signal strength of one target is fix, corresponding to the minimum value of each line. Shown are the results for JPDAF without (above) and with (below) exploitation of signal strength information.

ior. But for case 2, strong deviations are clearly visible: If the initial variance is too small, no convergence and thus no stable estimation is possible. As expected, larger values of Var_{ini} lead to better results. In both cases, obviously the signal strength estimation leads to slightly better results, if the target fluctuation model is Swerling-III. The reason for this might be the fact that the detection probability for Swerling-III is higher compared to Swerling-I for any given SNR_0, see Fig. 1, thus more detections are available to be processed.

In the second simulation scenario, the two targets move along the same trajectory for a considerable period of time, leading to a loss of identity in case of a traditional tracking algorithm. Here, the objective is to determine the capability of target discrimination with signal strength information in the final stage of the scenario. Based on the JPDAF algorithm and the simulation parameters given in Tab. 2, the results are plotted in Fig. 6 for Swerling-I and Fig. 7 for Swerling-III fluctuations, respectively, of the two targets. Shown is the probability for correct (solid lines) and incorrect (dashed lines) association of tracks with true targets at the final revisit for different signal strength combinations, based on the two fluctuation models. The signal strength of one target is fix, corresponding to the minimum value of each line. The upper plots correspond to target tracking without signal strength information. In this case, the signal strength only affects the true detection probability and thus the occurrence of target detections. As expected, for all combinations of the two targets'

signal strength the probability for correct association amounts to 50%. The lower plots illustrate the advantage of taking signal strength information into account: A clear performance gain in target discrimination is visible for both fluctuation models, with a stronger separation capability for larger differences in signal strength. Comparing the results in Figs. 6 and 7 (lower plots), apparently the discrimination performance of the algorithm is sligthly higher in case of Swerling-III. This is probably due to the distinct peak in the probability density of Swerling-III fluctuations, see Fig. 1, leading to a more obvious discrimination of the two signal strength distributions.

Table 1: Simulation parameters for scenario 1.

Monte Carlo runs	N_{MC}	=	1000
Target velocity	v_{target}	=	$15\,\mathrm{m/s}$
Process noise	σ_p	=	$0.5\,\mathrm{m/s^2}$
Range error	σ_r	=	$15\,\mathrm{m}$
Azimuth error	σ_φ	=	0.5
Mean false alarms	$\bar{n}_{FA}$	=	1
Field of view	$\lvert V\rvert$	=	$30\,\mathrm{km} \times 30\,\mathrm{km}$
Sensor position	$\vec{r}_{sensor}$	=	$[-5,-5,10]^\top\mathrm{km}$
Revisit rate	Δ_T	=	$2\,\mathrm{s}$
Detector threshold	λ	=	4
Mean target SNR	SNR_0	=	30
Mean clutter SNR	CNR_0	=	10
Scenario duration	N_{scan}	=	200

Table 2: Simulation parameters for scenario 2.

Monte Carlo runs	N_{MC}	=	1000
Target velocity	v_{target}	=	$15\,\mathrm{m/s}$
Process noise	σ_p	=	$0.5\,\mathrm{m/s^2}$
Range error	σ_r	=	$10\,\mathrm{m}$
Azimuth error	σ_φ	=	0.25
Mean false alarms	$\bar{n}_{FA}$	=	1
Field of view	$\lvert V\rvert$	=	$10\,\mathrm{km} \times 10\,\mathrm{km}$
Sensor position	$\vec{r}_{sensor}$	=	$[-1,5,10]^\top\mathrm{km}$
Revisit rate	Δ_T	=	$2\,\mathrm{s}$
Detector threshold	λ	=	4
Mean clutter SNR	CNR_0	=	10

5 Conclusions

In this paper we developed a tracking algorithm which incorporates signal strength information. In contrast to previous approaches, the knowledge on the target's signal strength is not only used for an improved calculation of the association probabilities, but it enters into the algorithm as a random variable which is sequentially estimated. Based on simulation scenarios, the performance of the presented algorithm is evaluated. As expected, the exploitation of signal strength leads to a performance gain in target discrimination in a multi-target scenario.
Further work will focus on the incorporation of signal strength information into the CPHD algorithm [10] and on a multiple model approach for different target fluctuation models.

References

[1] D. Lerro, and Y. Bar-Shalom, "Automated Tracking With Target Amplitude Information", *Proc. of American Control Conference*, San Diego, 1990.

[2] G. van Keuk, "Multihypothesis Tracking Using Incoherent Signal-Strength Information", *IEEE Trans. on Aerospace and Electronic Systems*, Vol. 32, No. 3, 1996.

[3] D. Clark, B. Ristic, Ba-Ngu Vo, and B.T. Vo, "Bayesian Multi-Object Filtering With Amplitude Feature Likelihood for Unknown Object SNR", *IEEE Trans. on Signal Processing*, Vol. 58, No. 1, pp. 26-37, 2010.

[4] P. Swerling, "Probability of Detection for Fluctuating Targets", *IRE Trans. on Information Theory*, Vol IT-6, pp. 269–308, April 1960.

[5] Y. Bar-Shalom, and X.-R. Li, *Estimation and Tracking: Principles, Techniques, and Software*, Artech House, Boston, 1993.

[6] Y. Bar-Shalom, and X.-R. Li, *Multitarget-Multisensor Tracking: Principles and Techniques*, YBS Publishing, Storrs, CT, 1995.

[7] W. Koch, "Tracking and Data Fusion Applications", *Advanced Radar Signal and Data Processing*, Educational Notes RTO-EN-SET-086, Paper 9, France, 2006.

[8] $\mathcal{N}(\mathbf{z};\mathbf{H}\,\mathbf{x},\mathbf{R})\;\mathcal{N}(\mathbf{x};\mathbf{y},\mathbf{P}) = \mathcal{N}(\mathbf{z};\mathbf{H}\,\mathbf{y},\mathbf{S})\;\mathcal{N}(\mathbf{x};\mathbf{y}+\mathbf{W}(\mathbf{z}-\mathbf{H}\,\mathbf{y}),\mathbf{P}-\mathbf{W}\mathbf{S}\mathbf{W}^\top)$ with $\mathbf{S}=\mathbf{H}\mathbf{P}\mathbf{H}^\top+\mathbf{R}$, $\mathbf{W}=\mathbf{P}\mathbf{H}^\top\mathbf{S}^{-1}$

[9] L. Devroye, *Non-Uniform Random Variate Generation*, Springer-Verlag, New York, 1986.

[10] R. Mahler, "A Theory of PHD Filters of Higher Order in Target Number", *IEEE Trans. on Aerospace and Electronic Systems*, 2007.